이 학 석 사 학 위 논 문

Surface-Enhanced Raman Scattering of Cyanide and Isocyanide: A Tool to Detect Electron Transfer

나이트릴 분자와 아이소나이트릴 분자의 표면 증강 라만 산란을 이용한 전자 이동 현상 고찰

2014 년 2 월

서울대학교 대학원

화학부 물리화학전공

이 승 훈

Surface-Enhanced Raman Scattering of Cyanide and Isocyanide: A Tool to Detect Electron Transfer

by Seung Hun Lee
Supervisor : Kwan Kim

A Thesis for the M. S. degree in Physical Chemistry

Department of Chemistry
Graduate School
Seoul National University

Feb. 2014

Abstract

We learned recently that the NC stretching peak of 2,6-dimethylphenylisocyanide (2,6-DMPI) is very susceptible to the surface potential of Au or Ag onto which 2,6-DMPI is assembled. The surface potential of Au or Ag nanoparticles is even subject to change by volatile organic compounds (VOCs), which can be monitored by the surface-enhanced Raman scattering (SERS) of 2,6-DMPI. We also learned recently that the cyanide anion is a better adsorbate than isocyanide. This is because the CN stretching frequency of the cyanide species varies by twice the amount of isocyanide in response to an external electric field and further, metal ions are able to bind to the pendant nitrogen lone pair of electrons of CN on Ag or Au, resulting in the shift of the C ≡ N stretching band by up to 60 cm^{-1}. On this basis, two different experiments have been carried out in this work, one titled "Au-to-CO Electron Transfer Evidenced by Surface-Enhanced Raman Scattering of 2,6-Dimethylphenylisocyanide" and the other titled "Fe^{3+} to Fe^{2+} Conversion by Plasmonically Generated Hot Electrons from Ag Nanoparticles: Surface-Enhanced Raman Scattering Evidence", hoping to raise the level of understanding on the charge-transfer occurring across the interface.

The observation made from "Au-to-CO Electron Transfer Evidenced by Surface-Enhanced Raman Scattering of 2,6-Dimethylphenylisocyanide" can be summarized as follows.

Au nanoparticles are known to be efficient CO oxidation catalysts under ambient conditions. Investigation of the interaction of CO with Au is difficult particularly using Raman spectroscopy. Although indirect, we demonstrate the transfer of electrons from Au to CO by means of surface-enhanced Raman scattering of 2,6-

dimethylphenylisocyanide, exploiting the susceptibility of the NC stretching band of isocyanide to the variation of the surface potential of Au nanoparticles. The back-bonding from Au to the CO 2_b orbital must be dominant over the 5 donation of CO to Au.

The observation made from "Fe^{3+} to Fe^{2+} Conversion by Plasmonically Generated Hot Electrons from Ag Nanoparticles: Surface-Enhanced Raman Scattering Evidence" can be summarized as follows.

We have demonstrated using surface-enhanced Raman scattering (SERS) of cyanide that "hot" electrons can be plasmonically generated from nanostructured Ag and/or Au substrates. For this, we first fabricated poly(ethylenimine) (PEI)-capped Ag and Au nanoparticle films onto glass slides. Cyanide was then adsorbed (via the carbon lone-pair electrons) onto the films to obtain the NC/Ag and NC/Au systems. Subsequently, Fe^{3+} or Fe^{2+} ions were bound to the pendant nitrogen atoms to obtain the corresponding Fe^{3+}/NC/Ag and Fe^{3+}/NC/Au systems or the Fe^{2+}/NC/Ag and Fe^{2+}/NC/Au systems. All these systems were stable under laser light illumination at 632.8-nm, with CN stretching bands at 2159 and 2143 cm^{-1} for the Fe^{3+}/NC/Ag and Fe^{2+}/NC/Ag systems, respectively, and at 2180 and 2158 cm^{-1} for the Fe^{3+}/NC/Au and Fe^{2+}/NC/Au systems, respectively. Under the laser light illumination at 514.5-nm, the Fe^{3+}/NC/Ag system was gradually converted to the Fe^{2+}/NC/Ag system, with the CN stretching band shifting from 2159 to 2143 cm^{-1}. This Fe^{3+} to Fe^{2+} conversion is due to the hot electrons plasmonically generated from the PEI-capped Ag nanoparticle film. Furthermore, it appears as though the generation of hot electrons is an efficient process, because Fe^{3+} to Fe^{2+} conversion was facile although the Fe^{3+}/NC/Ag system was buried in ice at the liquid N_2 temperature (77 K). In turn, the infeasible oxidation of Fe^{2+} to Fe^{3+} is due to the formation of so-called "hot" holes, which if generated, would be

reactive only to the species in contact with the Ag nanoparticles. Because the PEI-capped Au film was not SERS-active at 514.5-nm, the generation of hot electrons with excitation occurring at shorter wavelengths could not be examined, although the Fe^{3+}/NC/Au system could be converted to the Fe^{2+}/NC/Au system (or vice versa) by a brief contact with a mild solution of borohydride (or permanganate).

Key words: 2,6-Dimethylphenylisocyanide, Cyanide, Carbon Monoxide, Silver, Gold, Surface-Enhanced Raman Scattering (SERS), Surface Potential, Hot Electron, Plasmonics

Student Number: 2012-20284

Contents

Chapter 1. Au-to-CO Electron Transfer Evidenced by Surface-Enhanced Raman Scattering of 2,6-Dimethylphenylisocyanide

1.1. Introduction

Metal-oxide-supported Au nanoparticles are known to be highly efficient CO oxidation catalysts that are operative at and below room temperatures.[1-4] Extensive experimental and theoretical investigations have aimed to elucidate the origin of their reactivity, revealing that the key influential factors are the particle size of Au and the type of oxide support.[5-7] The optimum size of Au nanoparticles is reportedly ~3–4 nm[8], and transition-metal oxide supports (Fe, Ti, Ce) containing Au nanoparticles (~1 wt%) have been demonstrated to be more active for CO oxidation than main–group element oxides (Si, Mg. Sn)[9]. The proposed mechanisms for CO oxidation on Au nanoparticles can be divided into two categories: one involving solely the Au nanoparticle, whereas the other requires interaction with the oxide support. Kinetic studies show that CO and O_2 are adsorbed on the surface of Au until saturation is achieved, and the reaction of the adsorbed CO and O_2 is the rate-determining step.[10]

The adsorption energy of CO on noble metals is several degrees smaller than

that on usual metals.[11] Owing to the low adsorption strength, examination of the physicochemical properties of adsorbed species on Au under ambient conditions is exigent. Accordingly, the adsorption characteristics of CO on Au have generally been studied at temperatures in the range 100 ~ 135 K. At ambient temperatures, high CO coverage can be obtained by raising the CO gas pressure. Combined reflection-absorption infrared spectroscopy and scanning tunneling microscopy evaluation of CO adsorption on Au(110) at 300 K and CO pressures up to 500 torr was conducted by Jugnet et al.[12], revealing the presence of weakly chemisorbed CO with a C–O stretching frequency of ν_{CO} = 2110 cm^{-1} at pressures above 10^{-2} torr and another, possibly physisorbed, species with ν_{CO} = 2141 cm^{-1} at ≥ 100 torr.

Based on the Blyholder model of CO adsorption, electron transfer proceeds from the slightly antibonding CO 5σ orbital to the metal valence orbital, while the metal d-orbitals back-donate electrons to the strongly antibonding CO $2\pi_b$ orbital.[13] In all prior studies of CO on Au, the CO stretching band was observed to red-shift from ~2120 cm^{-1} to ~2110 cm^{-1} with increasing coverage.[14] In principle, the coverage dependence of the CO stretching band can be explained as the result of two offsetting effects, i.e., chemical interaction and dipolar coupling.[15,16] The red-shift is indicative of the dominance of a chemical interaction (with the

substrate) over a dipolar coupling (between adsorbates). The red-shift may also indicate that the back-bonding from Au to the CO $2\pi_b$ orbital dominates transfer from CO to Au. Experimental verification of whether electrons are transferred from CO to Au overall, or vice versa, is not facile, given that the interaction itself is very weak.

Recently, we demonstrated that a system of isocyanides adsorbed on nanostructured Au is very useful for the detection of volatile organic compounds (VOCs) by means of surface-enhanced Raman scattering (SERS), exploiting the variation in the NC stretching frequency, which changes by as much as 36 cm^{-1} per 1 V variation of the metal electrode.[17-22] Remarkably, the NC stretching band could be shifted by exposure to VOCs, even under non-electrochemical conditions.[19] An example of this is the observed blue-shift of the NC band from 2182 to 2188 cm^{-1} in the presence of gaseous acetone, as well as the red-shift from 2182 to 2162 cm^{-1} in the presence of ammonia.[19] These blue- and red-shifts correspond to changes in the surface potential of Au by +0.16 and -0.56 V, respectively, and are associated with either an s-type charge transfer from Au to the unoccupied p-orbital of the oxygen atom of acetone or the donation of the lone pair electrons on the ammonia nitrogen to the Au nanoparticles.[23,24] The present study demonstrates that the NC stretching band is blue-shifted as CO is exposed

to isocyanide-adsorbed Au nanostructures, suggesting that electrons are transferred from Au to CO.

1.2. Experimental

Chemicals. Au foil (0.05 mm thick, 99.99%) and 2,6-dimethylphenyl isocyanide (2,6-DMPI, 96%) were purchased from Sigma-Aldrich and used as received. Carbon monoxide (CO, ≥99.0%) and nitrogen (N_2, ≥99.0%) gases were purchased from Dongjin Company. Unless otherwise specified, all chemicals were reagent grade. Highly purified water with a resistivity greater than 18.0 MΩ·cm (Millipore Milli-Q system) was used for the preparation of the aqueous solutions.

Preparation of SERS-active Au Substrate. A SERS-active Au substrate (0.05 mm thick foil) was prepared via oxidation-reduction cycles (ORCs) in a 0.1M KCl solution by sweeping consecutively at 1 $V \cdot s^{-1}$ between -0.8 and +1.0 V versus a saturated Ag/AgCl electrode[25], and was then immersed partially or fully in a 1 mM ethanolic solution of 2,6-DMPI for 3 h. The 2,6-DMPI-adsorbed Au substrate was positioned inside a quartz cell and CO gas was set to flow through the cell at a flow rate of 100 $mL \cdot min^{-1}$ at atmospheric pressure. For potential-

dependent SERS measurements, a 2,6-DMPI-modified Au(ORC) substrate and a pure Pt wire were used as the working and counter electrodes, respectively, in a 0.1M $NaClO_4$. The potential of the electrochemical cell was controlled using a CH instruments model 660A potentiostat. All potentials are reported with respect to the saturated Ag/AgCl electrode. Before initiating any electrochemical measurement, the electrolyte solution was purged with high-purity N_2 gas.

Instrumentation. Raman spectra were obtained using a Renishaw Raman System 2000 spectrometer equipped with a holographic notch filter and an integral microscope (Olympus BH2-UMA). The 632.8 nm radiation from a 17 mW air-cooled He/Ne laser (Spectra Physics model 127) was used as the excitation source. Raman scattering was detected with 180° geometry using a Peltier-cooled (-70°C) CCD camera (400 × 600 pixels). The Raman band of a silicon wafer at 520 cm^{-1} was used to calibrate the spectrometer, and the accuracy of the spectral measurement was estimated to be better than 1 cm^{-1}. The typical laser power at the sampling position was 0.2 mW with an average spot size of 1 μm diameter. The integration time was 30 s.

1.3. Results and discussion

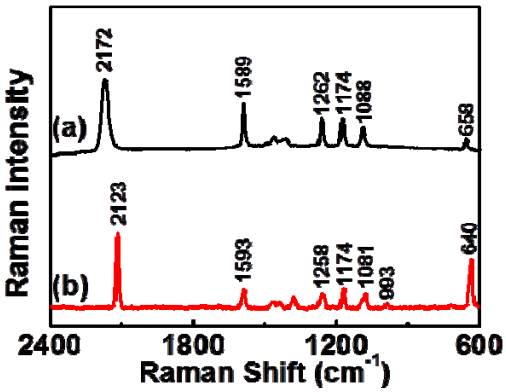

Figure 1. (a) SERS spectrum of 2,6-DMPI adsorbed on Au. (b) NR spectrum of 2,6-DMPI in neat state.

Initial attempts to measure the normal Raman (NR) spectrum of CO dissolved in water or ethanol, as well as the SERS spectrum of CO adsorbed on ORC-roughened Au, were unsuccessful. This can be understood by referring to the fact that the Henry's constant for CO in water at 25 °C is 9.71×10^{-4} mol·L^{-1}·atm^{-1}.[26] The concentration of CO in water under ambient conditions would thus be in the less than millimolar range. Such a low concentration generally cannot be detected via NR spectroscopy. Attempts to observe the Raman spectrum of CO on Au involved flowing pure CO gas over nanostructured Au, but no Raman peaks

appeared at around 2100 cm^{-1}. This suggests that the adsorption energy of CO on Au is not sufficiently large for detection of its presence by Raman spectroscopy. Only a limited number of molecules are expected to undergo weak interaction with the Au substrate. Although not directly detectable, evidence of their presence on Au could be derived from the NC stretching peak of isocyanides. We thus measured the SERS spectrum of 2,6-DMPI on Au in the absence and presence of CO.

Figure 1(a) shows the SERS spectrum of 2,6-DMPI adsorbed on an ORC-roughened Au. The acquired spectrum is consistent with that reported in an earlier publication. The SERS spectrum of 2,6-DMPI differs substantially from its NR spectrum shown in Figure 1(b). The most notable difference is associated with the NC group. The C–NC stretching band was considerably weakened, and shifted by as much as 18 cm^{-1} (from 640 to 658 cm^{-1}) upon adsorption on Au. The NC stretching peak was also blue-shifted by as much as 49 cm^{-1} (from 2123 to 2172 cm^{-1}). These observations can be understood by taking into account the antibonding character of the carbon lone-pair electrons in the isocyanide group.[21] The donation of these electrons to gold should increase the strength of the NC bond, resulting in the blue-shift of the NC stretching band.

Figure 2(a) shows a series of SERS spectra of 2,6-DMPI on Au measured under a flow of CO (at 100 $mL \cdot min^{-1}$ at 1 atm) (see Scheme 1). The CO stretching

peak was not at all apparent. Most peaks, except the NC stretching peak of 2,6-DMPI, remained unchanged throughout the spectral measurements. The NC stretching peak was, however, subject to change. The band gradually blue-shifted by 5 cm^{-1} from 2172 to 2177 cm^{-1} within 15 min, as summarized in Figure 2(b).

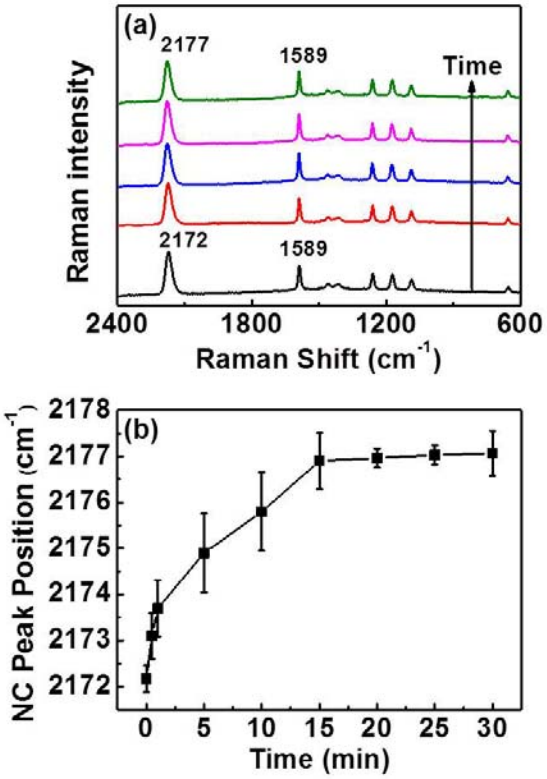

Figure 2. (a) SERS spectra of 2,6-DMPI on Au acquired under the flow of carbon monoxide (at 100 $mL \cdot min^{-1}$ at 1 atm). (b) Variations in NC stretching peak position with time of flow of CO in (a).

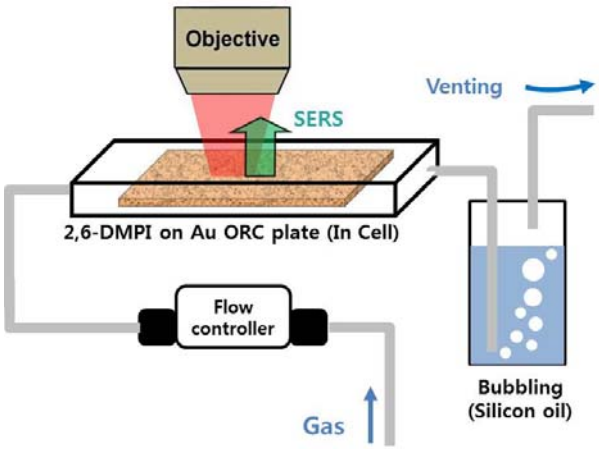

Scheme 1. Schematic diagram of protocol for determining effect of CO on NC stretching peak of 2,6-DMPI adsorbed on Au substrate.

The possibility of the direct interaction of CO with 2,6-DMPI is very low given that the NR spectrum of 2,6-DMPI in methanol is invariant when bubbled with CO. The blue-shift of the NC stretching band induced by CO is thus deduced to be indirect. In our recent study[19], a similar blue-shift of 6 cm^{-1} was observed when acetone vapor was streamed over 2,6-DMPI on Au. In the presence of flowing ammonia vapor, the NC stretching band was red-shifted by as much as 20 cm^{-1}. These blue- and red-shifts were interpreted in terms of an s-type charge transfer from Au to the unoccupied p–orbital of the oxygen atom of acetone and the donation of the lone-pair electrons of the ammonia nitrogen to Au nanoparticles, respectively.[23,24]

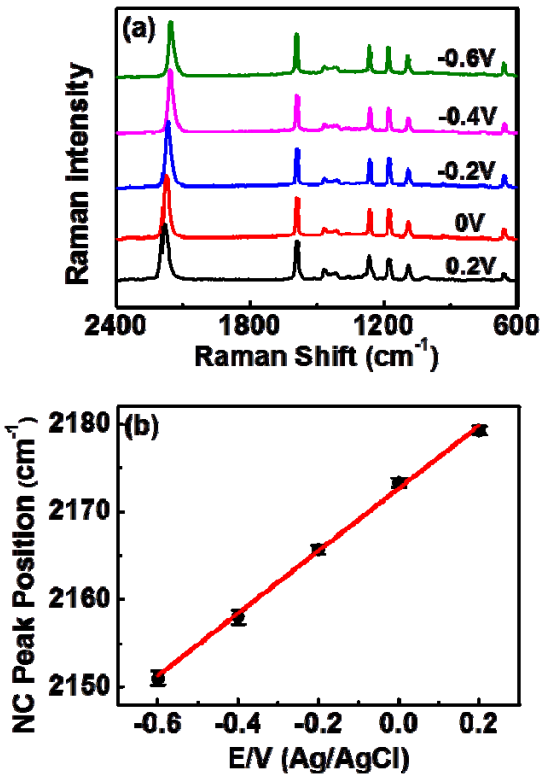

Figure 3. (a) Potential-dependent SERS spectra of 2,6-DMPI on an Au (ORC) electrode in 0.1 M $NaClO_4$ aqueous solution. (b) Position of the NC stretching peak of 2,6-DMPI on Au drawn versus the applied potential in (a). The error bars indicate one standard deviation of three independent measurements.

Figure 3(a) shows a series of potential-dependent SERS spectra of 2,6-DMPI adsorbed on an ORC-roughened Au electrode in the potential region between +0.2 and -0.6 V in 0.1 M $NaClO_4$ aqueous solution. It was seen that the relative peak

intensities as well as peak positions of the ring modes were invariant with respect to the potential variation. In contrast with the ring modes, noticeable peak shift was observed for the NC stretching band. The NC stretching peak was gradually blue-shifted following the increase in the surface potential. This can be understood by referring to the bonding scheme of 2,6-DMPI to Au. As the potential is made more positive, there is increased σ donation from the C atom to the metal, resulting in the increase in the bond order and thus the vibrational frequency of the NC bond. The opposite will take place when the potential is made more negative. It has also to be considered that back-donation from the metal to the NC π^* orbitals can occur at negative potentials, decreasing the bond order and vibrational frequency. Because of these effects, the NC stretching peaks are observed at 2180, 2173, 2165, 2159, and 2151 cm^{-1} at +0.2, 0.0, -0.2, -0.4, and -0.6 V, respectively. As can be seen in Figure 3(b), these values vary linearly with a slope of ca. 36 $cm^{-1} \cdot V^{-1}$; this result is the same as in our previous study.[19] The blue-shift of NC stretching peak of 5 cm^{-1} observed herein when CO was flowed over 2,6-DMPI on Au corresponds to a potential change of +0.13 V.

In a prior surface-enhanced infrared absorption spectroscopy based study of CO on Au, the C≡O stretching peak was reported to appear at ~2120 cm^{-1}.[12] However, as described above, the SERS spectrum of CO was not observed herein.

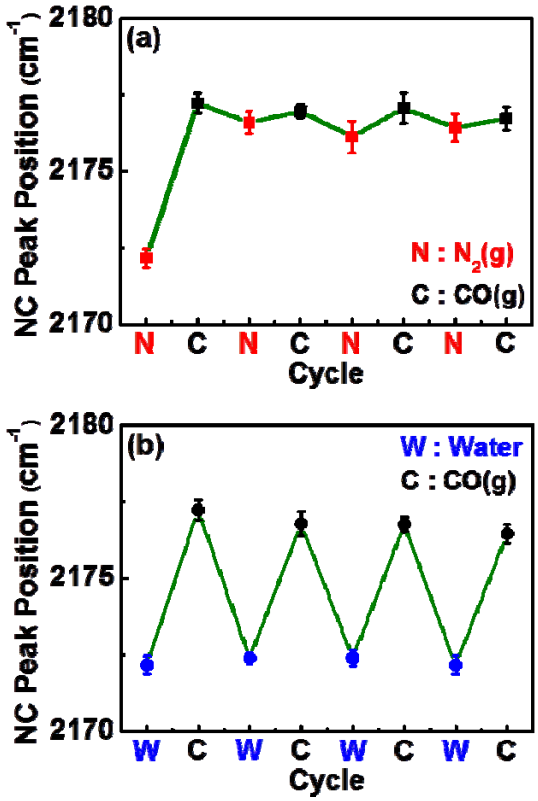

Figure 4. Variations in NC stretching peak position of 2,6-DMPI on Au (a) under alternate flows of CO and N_2 and (b) under the flow of CO and subsequent washing with water. The error bars indicate one standard deviation of five independent measurements.

Furthermore, only a limited number of CO could be adsorbed on Au, especially when the Au substrate was initially covered with 2,6-DMPI. Although not detectable by SERS, CO must, however, have affected the surface property of

the Au nanostructures. The blue-shift observed in Figure 2(b) suggests that electrons were transferred from Au to CO, increasing the surface potential of the Au substrate. It is notable that once blue-shifted by CO, the NC stretching peak remained unchanged even under a flow of N_2, as shown in Figure 4(a). This might indicate that a small quantity of CO was firmly adsorbed on the Au substrate. The high-energy sites such as kinks or steps not occupied by 2,6-DMPI are the most probable sites for CO chemisorption. However, the NC stretching peak returned to the original position when the CO-exposed substrate was washed with water, as shown in Figure 4(b).

The CO-induced blue-shift of the NC stretching peak of 2,6-DMPI on Au in Figure 2(a) is very intriguing given that the number of free sites available for the adsorption of CO is expected to be quite few when the Au substrate is initially fully covered with 2,6-DMPI. If more free sites were available for CO, the NC stretching peak of 2,6-DMPI should be affected to a greater extent. To verify this effect, we repeated the SERS measurements by initially introducing 10% surface coverage of the Au substrate with 2,6-DMPI, leaving the remaining surface free for adsorption of CO. In this case, the NC stretching peak was, in fact, blue-shifted by as much as ~9 cm^{-1}. The extent of the blue-shift observed here is almost twice that in Figure 2(a). The value is an asymptotic limit, given that no further shift was detected by variation of the number of free sites for CO. Based on the

potential-dependent SERS of 2,6-DMPI on Au as shown in Figure 3, the blue-shift of 9 cm^{-1} corresponds to a potential change of +0.25 V, that is, the surface potential of Au must increase by as much as +0.25 V upon exposure to CO under atmospheric pressure at ambient temperature. Thus, some electrons must move from Au to CO.

1.4. Summary and conclusion

Although CO adsorbed on Au could not be directly detected using Raman scattering spectroscopy, the presence of CO on Au was, nevertheless, successfully identified by exploiting the SERS of 2,6-DMPI. Exposure of the 2,6-DMPI-adsorbed Au substrate to CO induced a blue-shift of the NC stretching band by as much as 9 cm^{-1} under atmospheric pressure at ambient temperature. Based on the potential-dependent SERS of 2,6-DMPI on Au, the blue-shift of 9 cm^{-1} corresponds to a change in the surface potential of +0.25 V. This increase in the surface potential of Au suggests that electrons are transferred from Au to CO, indicating that back-donation from Au to the $2\pi_b$ orbital of CO must be dominant over the 5σ donation of CO to Au. The blue-shift of the NC stretching peak could not be reversed simply by flushing with N_2 gas, indicating that the adsorption

energy of CO on Au was higher than that of N_2 on Au. The NC stretching peak was, however, restored to the original position by washing the substrate with water. This work clearly demonstrates that isocyanide SERS can be exploited as an invaluable tool in the investigation of molecules that undergo weak interactions with SERS-active substrates such as Au.

1.5. References

(1) Fierro-Gonzalez, J.C.; Bhirud, V.A.; Gates, B.C., *Chem. Commun.* **2005,** *18,* 5275.

(2) Pillai, U.R.; Deevi, S., *Appl. Catal. B: Environ.* **2006,** *64,* 146.

(3) Carabineiro, S.A.C.; Bogdanchikova, N.; Avalos-Borja, M.; Pestryakov, A.; Tavares, P.B.; Figueiredo, J.L., *Nano Res.* **2010,** *4,* 180.

(4) Boccuzzi, F.; Chiorino, A,; Tsubota, S.; Haruta, M., *J. Phys. Chem.* **1996,** *100,* 3625.

(5) Haruta, M., *J. New. Mat. Electrochem.* Syst. **2004,** *7,* 163.

(6) Zheng, N.F.; Stucky, G.D., *J. Am. Chem. Soc.* **2006,** *128,* 14278.

(7) Remediakis, I.N.; Lopez, N.; Norskov, J.K., *Appl. Catal. A: Gen.* **2005,** *291,* 13.

(8) Valden, M.; Lai, X.; Goodman, D.W., *Science* **1998,** *281,* 1647.

(9) Gasior, M.; Grzybowska, B.; Samson, K.; Ruszel, A.; Haber, J., *Catal. Today* **2004,** *91-92,* 131.

(10) Gavril, D.; Georgaka, A.; Karaiskakis, G., *Molecules* **2012,** *17,* 4878.

(11) Gajdos, M.; Eichler, A.; Hafner, J., *J. Phys.: Condens. Matter.* **2004,** *16,* 1141.

(12) Jugnet, Y.; Aires, F.J.C.S.; Deranlot, C.; Piccolo, L.; Bertolini, J.C., *Surf. Sci.* **2002,** *521,* L639.

(13) Blyholder, G., *J. Phys. Chem.* **1964,** *68,* 2772.

(14) Meier, Douglas C.; Bukhtiyarov, V.; Wayne Goodman, D., *J. Phys. Chem. B* **2003,** *107,* 12668.

(15) Hollins, P.; Pritchard, J.; *Surf. Sci.* **1979,** *89,* 486.

(16) Woodruff, D.P.; Hayden, B.E.; Prince, K.; Bradshaw, A.M., *Surf. Sci.* **1982,** *123,* 397.

(17) Shin, D.; Kim, K.; Shin, K.S., *Chem. Phys. Chem.* **2010,** *11,* 83.

(18) Kim, K.; Kim, K.L.; Choi, J.Y.; Shin, K.S., *Phys. Chem. Chem. Phys.* **2011,** *13,* 5981.

(19) Kim, K.; Kim, K.L.; Shin, D.; Lee, J.W.; Shin, K.S., *Chem. Commun.* **2010,** *46,* 3753.

(20) Kim, K.; Shin, D.; Kim, K.L.; Shin, K.S., *J. Raman. Spectrosc.* **2012,** *43,* 1427.

(21) Kim, K.; Lee, J.W.; Shin, K.S., *Spectrochim. Acta A* **2013,** *100,* 15.

(22) Kim, K.; Lee, J.W.; Shin, D.H.; Choi, J.Y.; Shin, K.S., *Analyst* **2012,** *137,* 1930.

(23) Shafai, G.S.; Shetty, S.; Krishnamurty, S.; Shah, V.; Kanhere, D.G., *J. Chem. Phys.* **2007,** *126,* 14704.

(24) Wasileski, S.A.; Koper, M.T.M.; Weaver, M.J., *J. Am. Chem. Soc.* **2002,** *124,* 2796.

(25) Liu, Y.C., *Langmuir* **2002,** *18,* 174.

(26) Meadows, R.W.; Spedding, D. J., *Tellus* **1974,** *26,* 143.

Chapter 2. Fe^{3+} to Fe^{2+} Conversion by Plasmonically Generated Hot Electrons from Ag Nanoparticles: Surface-Enhanced Raman Scattering Evidence

2.1. Introduction

The term "hot electron" was originally introduced to describe non-equilibrium electrons (or holes) with an elevated effective temperature in semiconductors.[1] Because of their greater energy, hot electrons can tunnel out of semiconductor materials, leading to increased leakage current and/or damaging the encasing dielectric material, if the hot carrier disrupts the atomic structure of the dielectric. In semiconductors, hot electron effects are well known even at room temperature, although hot electrons generally arise at low temperatures.[2] Because of their smaller carrier density relative to metals, power is dissipated in a relatively small number of carriers in semiconductors, allowing the temperature to increase to a much greater extent. In semiconductors, hot electrons can also be generated via electromagnetic radiation.[3] if the electrons receive enough energy from light to leave the valence band (surpassing the conduction band), they

become hot electrons.

In metals, the large carrier density makes the hot electron effects less pronounced at room temperature.[4-7] Accordingly, the hot electron effects in metals have been observed at low temperatures. However, as in semiconductors, hot electrons can be generated via plasmonic resonances, even at room temperature.[8-15] If hot electrons were ejected out of a metallic substrate, positively charged holes would be left on the surface.[16] The hot electrons would be able to reduce the adsorbate assembled on the metal, while the holes could potentially oxidize the adsorbate.[17-19] The room temperature photodissociation of H_2 on Au/TiO_2 nanocomposites has been interpreted by Mukherjee et al. as being due to the plasmonically generated hot electrons.[20] On the other hand, the surface-enhanced Raman scattering (SERS) spectrum of 4-nitrobenzenethiol (4-NBT) on nanostructured Ag was observed to be similar to that of 4-aminobenzenethiol.[21-24] This spectral similarity could indicate that the nitro group of 4-NBT can be reduced by hot electrons plasmonically created from Ag.

The purpose of this work is to demonstrate, by means of SERS, that hot electrons are plasmonically generated from nanostructured Ag and/or Au, by illustrating that the chemical species on nanostructured Ag and/or Au can be reduced and/or oxidized by visible light. The model systems that have been examined in this study are comprised of cyanide-adsorbed nanostructured Ag and

Au, in which Fe^{2+} or Fe^{3+} ions are bonded to the pendant nitrogen lone-pair electrons of the cyanide species.[25] We have recently found that the CN stretching frequency of cyanide on Au is very susceptible to change when binding with metal cations via the pendant nitrogen atom.[26] Thus, we have examined the possibility of the reduction of Fe^{3+} to Fe^{2+} and/or the oxidation of Fe^{2+} to Fe^{3+} by monitoring the SERS peak of the CN stretching band. Neither conversion was evident from the nanostructured Au, but the reduction of Fe^{3+} to Fe^{2+} took place using only visible light when Fe^{3+} ions were bonded to the CN on Ag via the nitrogen lone-pair, implying that the nanostructured Ag must be a plasmonically efficient hot electron emitter.

2.2. Experimental

Chemicals. Hydrogen tetrachloroaurate ($HAuCl_4$, 99.99%), silver nitrate ($AgNO_3$, 99.8%), branched poly(ethylenimine) (PEI, MW ~25 kDa), benzenethiol (BT, 99+%), potassium cyanide (KCN, 96%), sodium borohydride ($NaBH_4$, 99%), and potassium permanganate ($KMnO_4$, 99+%) were purchased from Aldrich, and were used as received. Other chemicals, unless specified, were

reagent-grade. Highly purified water, with resistivity greater than 18.0 MΩ·cm (Millipore Milli-Q System), was used in preparing aqueous solutions.

Preparation of SERS-Active Au and Ag Films. To prepare PEI-stabilized Au nanoparticles, 25 mL of 1.4-mM aqueous $HAuCl_4$ solution was mixed with 0.7 mL of 1% (w/w) aqueous PEI, and stirred vigorously at 80 °C for 2 h. The PEI-stabilized Ag nanoparticles were prepared by boiling a mixture of 100 mL of 10-mM $AgNO_3$ and 1 mL of 2% (w/w) PEI for 15 min. As determined by transmission electron microscopy (TEM) analyses, the average sizes of the Au and Ag nanoparticles were 27 ± 7 and 19 ± 9 nm, respectively (with both types of nanoparticles being spherically shaped). Subsequently, toluene (2 mL) was poured over the PEI-stabilized Au (Ag) sol (5 mL), and BT (1.0 mL) was added into the toluene phase. Once this was completed, a fairly homogeneous Au (Ag) film was formed at the toluene-water interface. A large 2-dimensional (2-D) Au (Ag) film was also formed on a separate glass or mica substrate immersed in the mixture. For depositing Au (Ag) onto the inner walls of a capillary, the mixture was injected using a syringe through the capillary tube. BT was desorbed from the PEI-capped Au (Ag) nanoparticles without disturbing the SERS activity of the Au (Ag) film, via treatment with a 0.1M borohydride solution for 30 min. After the

complete disappearance of the BT peaks by SERS, the PEI-capped Au (Ag) film was washed with copious amounts of ethanol and then dried with nitrogen.

Instrumentation. The rate of flow through the capillary tubes was controlled using a Sage Instruments model 341 syringe pump. TEM images were taken on a JEM-200CX transmission electron microscope at 200 kV. Raman spectra were obtained using a Renishaw Raman system model 2000 spectrometer. The 514.5-nm line from a 20-mW Ar^+ laser (Melles-Griot model 351MA520), the 488- and 568-nm lines from a 20-mW Ar^+/Kr^+ laser (Melles-Griot Model 35KAP431), or the 632.8-nm line from a 17 mW He/Ne laser (Spectra Physics model 127) were used as the excitation sources. Raman scattering was detected over 180° with a Peltier-cooled (-70°C) charge-coupled device (CCD) camera (400 × 600 pixels). The Raman band of a silicon wafer at 520 cm^{-1} was used to calibrate the spectrometer.

2.3. Results and discussion

SERS-active Ag and Au substrates can be prepared using a variety of methods.[27-31] Herein, we used the PEI-capped Ag and Au nanoparticle films as the SERS substrates, primarily because of their high SERS-activity, stability against

cyanide etching, and ease of preparation and processing. We have recently found that PEI can simultaneously function as a reducing and stabilizing agent to form amine-functionalized Ag and Au nanoparticles.[32-36] The PEI-capped Ag and Au nanoparticles prepared in the aqueous phase can be assembled into 2-D arrays not only at the aqueous/toluene interface, but also at the inner surface of the sampling bottle via the addition of BT. Ag and Au nanoparticle films can also be formed, through a brief contact with the mixture, on the glass slides, the inner walls of capillary tubes, or even on the dielectric beads and cotton fabrics.[37] These Ag and Au films are highly SERS-active, showing very intense Raman peaks for BT, as shown in Figure 1(a). BT can be removed from the surfaces of Ag and Au, while still maintaining the SERS activity, by treating the films with a 0.1-M borohydride solution for 30 min.[32-33] Figures 1(b) and 1(c) show the Raman spectra obtained after the removal of BT, and after soaking the PEI-capped Ag and Au nanoparticle films in 1-mM ethanolic KCN for 10 min, respectively. The distinct peaks at 2132 cm^{-1} in Figure 1(b) and 2120 cm^{-1} in Figure 1(c) are due to the CN stretching band of the cyanide species adsorbed onto the PEI-capped Ag and Au nanoparticle films: hereafter, they will be represented as the NC/Ag and NC/Au systems. The CN stretching band of KCN dissolved in ethanol is observed at 2074 cm^{-1}, as shown in Figure 1(d). Hence, the CN stretching band of the cyanide species is blue-shifted by 58 and 46 cm^{-1}, respectively, upon adsorption on the PEI-capped

Ag and Au nanoparticle films. The origin of such large blue-shifts is associated with the anti-bonding character of the carbon lone-pair from the cyanide species.[38-40] The donation of anti-bonding electrons from the carbon atom to silver and gold during surface adsorption (forming either Ag–CN or Au–CN) results in a significant blue-shift of the CN stretching band.[41]

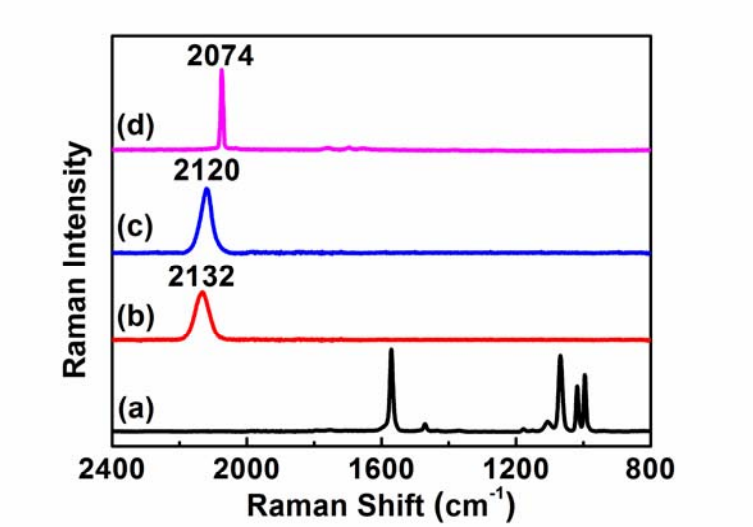

Figure 1. (a) SERS spectrum of BT adsorbed onto a PEI-capped Ag nanoparticle film in a prepared state. SERS spectra of cyanide adsorbed onto PEI-capped (b) Ag and (c) Au nanoparticle films. (d) Normal Raman spectrum of KCN dissolved in ethanol. All spectra were obtained using 632.8-nm radiation as the excitation source.

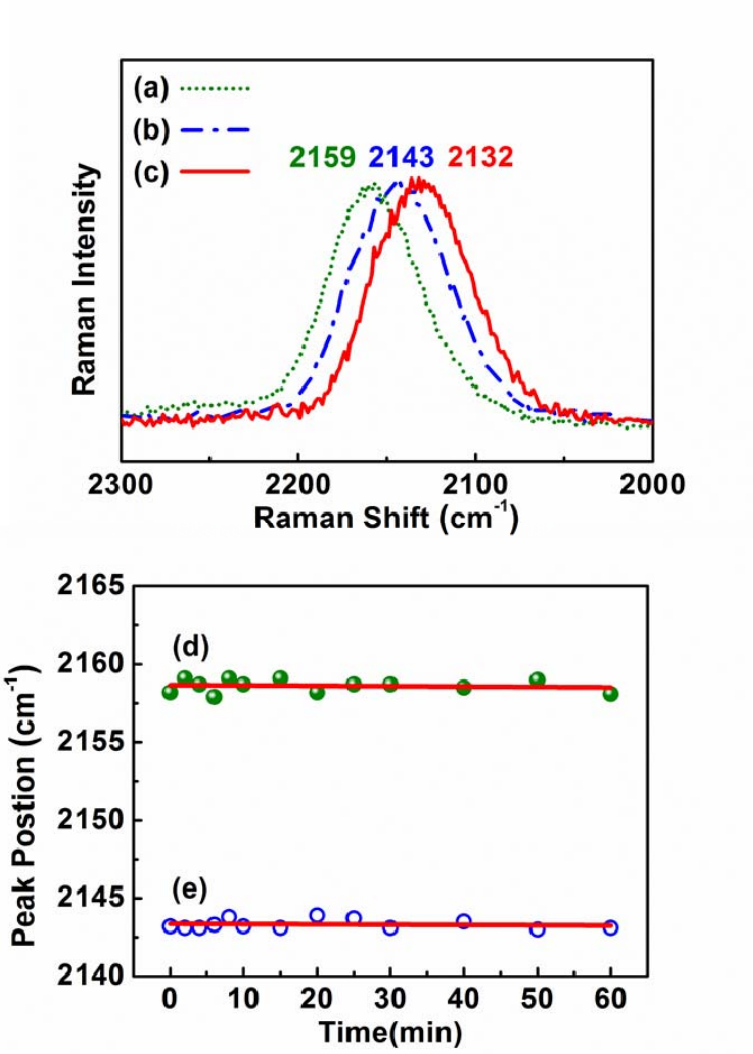

Figure 2. SERS spectra of the (a) Fe^{3+}/NC/Ag and (b) Fe^{2+}/NC/Ag systems measured using 632.8-nm radiation as the excitation source. (c) SERS spectrum of NC/Ag (reproduced from Figure 1(b)). The peak positions of the CN stretching bands in (a) and (b) are drawn in (d) and (e), respectively, against the measurement time.

The nitrogen atom of the NC/Ag and NC/Au systems can form a dative bond with transition metal ions such as Fe^{3+} and Fe^{2+}. This binding is favorable not only thermodynamically, but kinetically as well.[26] Accordingly, in this work, the NC/Ag and NC/Au systems were first soaked in 0.1-mM ethanolic solution of $Fe(NO_3)_3$ or $Fe(NO_3)_2$ for 30 s and then washed with ethanol: $Fe(NO_3)_3$ can etch Ag according to the equation of $Ag(s) + Fe(NO_3)_3(aq) \rightarrow AgNO_3(aq) + Fe(NO_3)_2(aq)$,[42] so the immersion time is set for 30 s. Hereafter, the NC/Ag and NC/Au systems treated with a solution of Fe^{3+} or Fe^{2+} ions will be labeled as the Fe^{3+}/NC/Ag and Fe^{3+}/NC/Au systems, respectively, or the Fe^{2+}/NC/Ag and Fe^{2+}/NC/Au systems, respectively. Figures 2(a) and 2(b) show the Raman spectra of the Fe^{3+}/NC/Ag and Fe^{2+}/NC/Ag systems, respectively, measured using 632.8-nm radiation as the excitation source. The CN stretching bands were invariant with time, at least under illumination at 632.8-nm (the laser power at the sampling position was 2.1 mW). The CN stretching bands were located at 2159 cm^{-1} for the Fe^{3+}/NC/Ag system (Figure 2(a)), and 2143 cm^{-1} for the Fe^{2+}/NC/Ag system (Figure 2(b)). Upon comparison with the data presented in Figure 1(b) (also reproduced in Figure 2(c)), the CN stretching band has blue-shifted by 27 and 11 cm^{-1}, respectively, as Fe^{3+} and Fe^{2+} ions are bound to the nitrogen lone-pair electrons of the CN on Ag. The CN bond became stronger as Fe^{3+} and Fe^{2+} ions

were bonded to the nitrogen atom of the NC/Ag system because of the anti-bonding lone-pair electrons of nitrogen. These electrons were donated far more to the Fe^{3+} than to the Fe^{2+} ions.[25-26] The invariance of the CN stretching bands with time in Figures 2(a) and 2(b) (also see Figures 2(d) and 2(e)) seems to indicate that the hot electrons, as well as the hot holes, were not generated from the PEI-capped Ag nanoparticles, but from light at 632.8-nm (at least at a power lower than 2.1 mW).

We subsequently obtained the Raman spectra of the Fe^{3+}/NC/Ag and Fe^{2+}/NC/Ag systems using 514.5-nm radiation as the excitation source. Figures 3(a) and 3(b) show a series of CN stretching bands observed as a function of time under the illumination of 514.5-nm radiation for the Fe^{3+}/NC/Ag and Fe^{2+}/NC/Ag systems, respectively (the laser power at the sampling position was again 2.1 mW). For the Fe^{2+}/NC/Ag system, the CN stretching band was observed at 2143 cm^{-1} (as shown in Figure 3(b)); however, for the Fe^{3+}/NC/Ag system, the CN stretching band was observed initially at 2159 cm^{-1} and was then red-shifted gradually toward 2143 cm^{-1} (as shown in Figure 3(a)). Clearly, the Fe^{3+} ions bonded to the NC/Ag system were reduced to Fe^{2+} ions by 514.5-nm light. This is certainly due to hot electrons plasmonically generated from the PEI-capped Ag nanoparticles. The infeasible oxidation of Fe^{2+} to Fe^{3+} could be rationalized using the argument that hot holes, if generated, would be reactive only toward the

species in contact with the Ag nanoparticles. The peak positions of the CN stretching band in Figure 3(a) measured as a function of time are collectively plotted in Figure 3(c). The time variation appears to be exponential, so it is tempting to fit them using an exponential function.

The CN stretching bands in Figure 3(a) must have been contributed by the newly-formed Fe^{2+}/NC/Ag system, as well as the unreacted Fe^{3+}/NC/Ag system. Accordingly, each measured band in Figure 3(a) has been resolved into two components, one from the Fe^{3+}/NC/Ag system centered at 2159 cm^{-1} and the other from the Fe^{2+}/NC/Ag system centered at 2143 cm^{-1}, as illustrated in Figure 4(a). Figures 4(b) and 4(c) show the variation in the CN stretching band intensity of the Fe^{3+}/NC/Ag and Fe^{2+}/NC/Ag systems, respectively. For the data in Figure 4(b), we selected the best fitting exponential, $[Fe^{3+}] = [Fe^{3+}]_o \exp(-kt)$, and determined the associated rate constant k. To better characterize the rate constant, the laser power dependence was examined using a 514.5-nm laser. The Fe^{3+} to Fe^{2+} conversion was exponential at three laser powers (1.05, 1.58, and 2.1 mW), and was faster when the laser power was increased. Figure 4(d) shows the calculated rate constants versus the laser power used. Although the number of data points in Figure 4(d) is not large, it is evident that the rate constant is almost linearly proportional to the laser power. This could mean that there was no multiphoton excitation in the experiment.

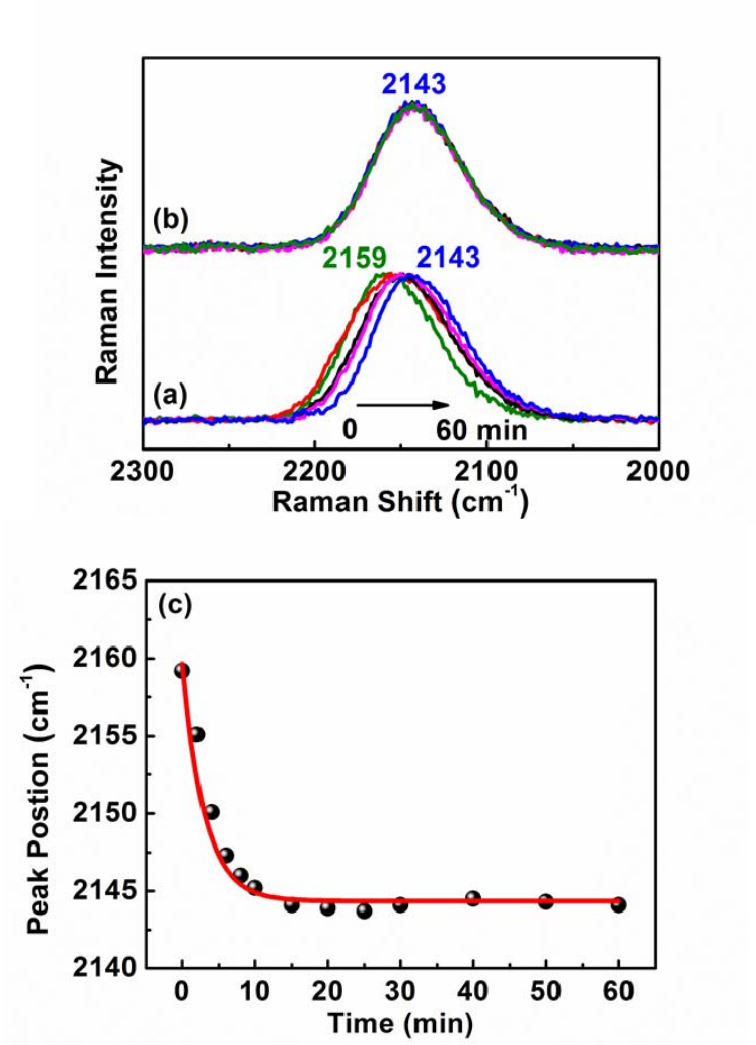

Figure 3. SERS spectra of (a) the Fe^{3+}/NC/Ag and (b) the Fe^{2+}/NC/Ag system measured using 514.5-nm radiation. (c) The peak position of the CN stretching band in (a) drawn versus the measurement time.

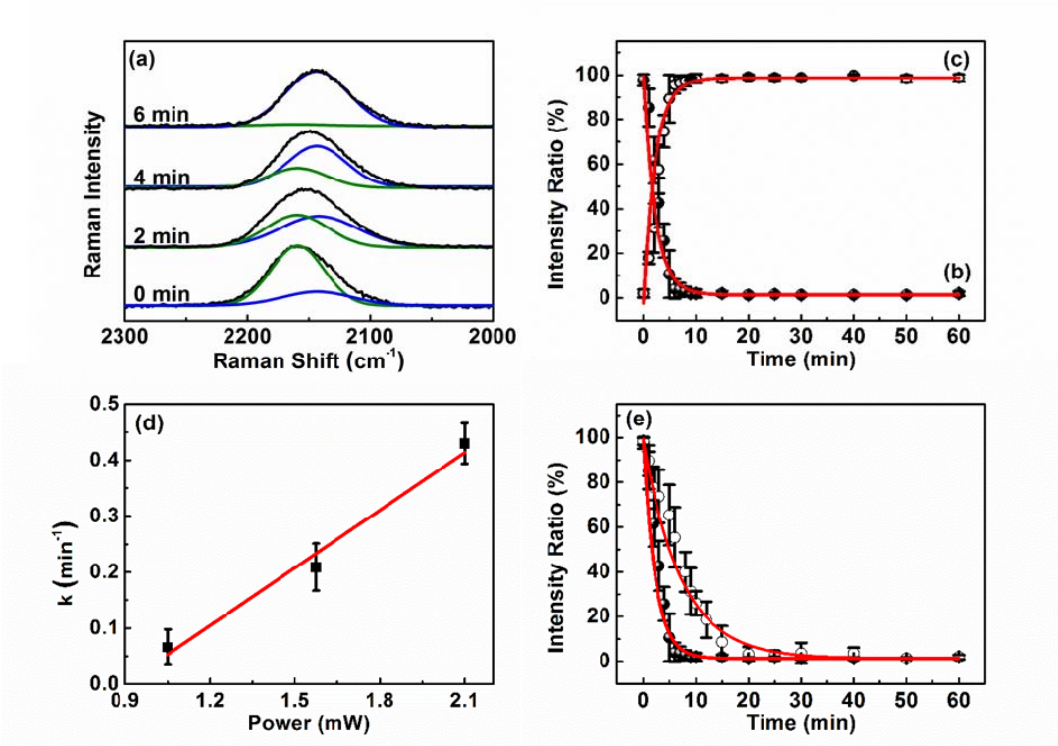

Figure 4. (a) Deconvolutions of the CN stretching bands of the Fe^{3+}/NC/Ag system at 0, 2, 4, and 6 min in Figure 3(a) into two components, one due to the Fe^{3+}/NC/Ag system and the other due to the Fe^{2+}/NC/Ag system. Variation of the CN stretching band intensity with time in (a), due to (b) the Fe^{3+}/NC/Ag system and (c) the Fe^{2+}/NC/Ag system. (d) Rate constant, k, in $[Fe^{3+}] = [Fe^{3+}]_o \exp(-kt)$ determined at three different laser powers at 514.5-nm excitation. (e) Comparison of the variations of the CN stretching band intensity of the Fe^{3+}/NC/Ag system with time at liquid N_2 temperature (77 K) (open circles) and at room temperature (solid circles) (the laser power at the sampling position was the same at both temperatures). See text. All error bars indicate the average and standard deviation of 3 different measurements.

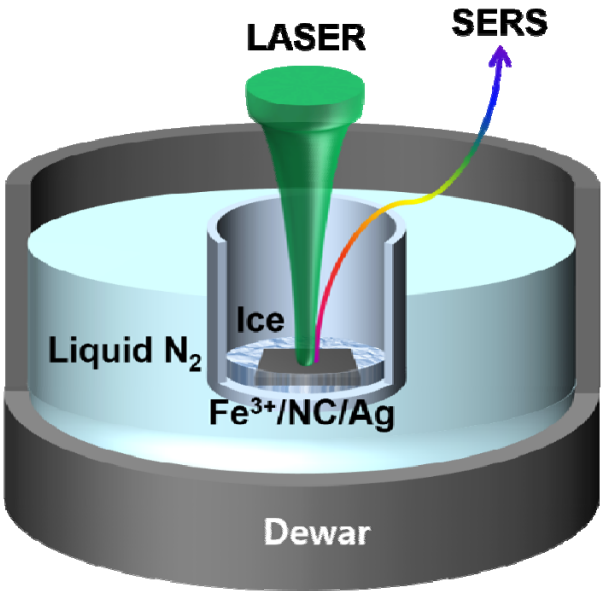

Scheme 1. Experimental arrangement used to measure the SERS spectrum of Fe^{3+}/NC/Ag in ice at liquid N_2 temperature (77 K).

To obtain additional information regarding the rate constant, we obtained the Raman spectrum of the Fe^{3+}/NC/Ag system buried in ice at 77 K (the temperature of liquid nitrogen; see Scheme 1 for the experimental configuration). To our amazement, we found that the reduction of Fe^{3+} to Fe^{2+} took place even at this low temperature. The variation in the CN stretching band intensity for the Fe^{3+}/NC/Ag system at both 77 K and at room temperature is shown in Figure 4(e). The laser power at the sampling position was the same at both temperatures, and confirmed separately using a power meter. The Fe^{3+} to Fe^{2+} conversion is slightly slower at 77 K than at room temperature. The activation energy (E_a) can be obtained from a

plot of ln k versus 1/T; from the k values obtained at 77 K and at room temperature, the E_a value was determined to be 1.0 kJ/mol. This value is quite small, especially when compared with the activation energies of typical chemical reactions, suggesting that the plasmonic generation of hot electrons from the PEI-capped Ag nanoparticles is an efficient process.

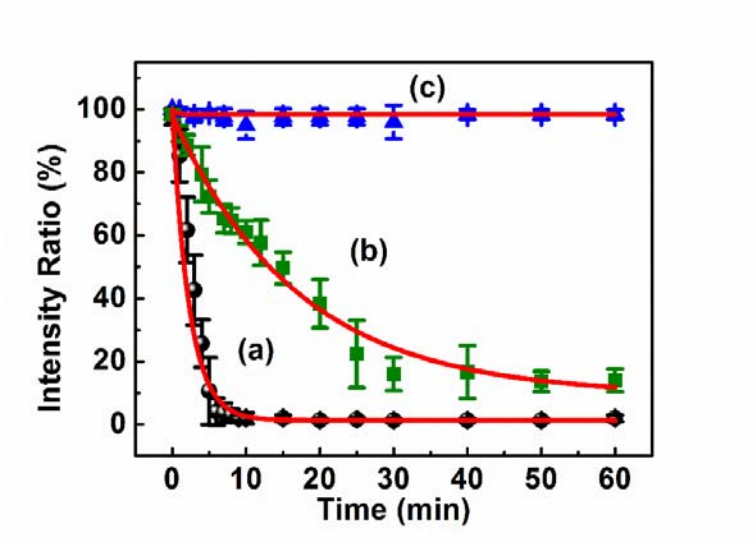

Figure 5. Comparison of the variations of the CN stretching band intensity of the Fe^{3+}/NC/Ag system with time (at the same power of ~2.1 mW) with excitation at (a) 514.5-, (b) 568-, and (c) 632.8-nm. The error bars indicate the average and standard deviation of 3 different measurements.

Fe^{3+} to Fe^{2+} conversion was more facile when excitation occurred at shorter wavelengths. Unfortunately, the laser power at 488-nm was not strong enough to make a quantitative measurement using the experimental conditions employed

herein. As described earlier, no Fe^{3+} to Fe^{2+} conversion was identified using 632.8-nm as the excitation source. At 568-nm excitation, the Fe^{3+} to Fe^{2+} conversion took place; however, the rate of conversion at 568-nm was lower than that at 514.5-nm. Under our experimental conditions, the conversion of the Fe^{3+}/NC/Ag system to the Fe^{2+}/NC/Ag system was not complete even after an hour of 568-nm excitation. This is shown in Figure 5, in which the Fe^{3+} to Fe^{2+} conversion (observed at the same power) at the 514.5-nm excitation, as well as the invariance at the 632.8-nm excitation, are shown for comparison. Thus, we believe that the conversion of Fe^{3+} to Fe^{2+} is more facile when excitation occurs at shorter wavelengths than when the excitation occurs at longer wavelengths.

Figures 6(a) and 6(b) show the Raman spectra of the Fe^{3+}/NC/Au and Fe^{2+}/NC/Au systems, respectively, measured using 632.8-nm radiation as the excitation source. The CN stretching band appeared at 2180 cm^{-1} when Fe^{3+} was bonded to the CN on Au, and at 2158 cm^{-1} when Fe^{2+} was bonded to the CN on Au. Comparing these stretches with that from Figure 1(c), the CN stretching band has blue-shifted by 60 and 38 cm^{-1} as Fe^{3+} and Fe^{2+} ions were bonded to the cyanide on Au, respectively. However, as with the Ag system, the CN stretching peaks were invariant with time under the illumination of 632.8-nm light. This would indicate that the plasmonically induced photoexcitation of hot electrons (which reduce Fe^{3+} to Fe^{2+}), as well as hot holes (which oxidize Fe^{2+} to Fe^{3+}), did

not occur with 632.8-nm light in the cyanide-adsorbed, PEI-capped Au nanoparticle film. Because the PEI-capped Au nanoparticle film was not SERS-active at wavelengths lower than 632.8-nm, we were unable to verify whether hot electrons could be generated from Au nanoparticles using a laser light at lower wavelengths. However, the Fe^{3+}-bonded CN system on Au can be reduced chemically to the Fe^{2+}-bonded CN system on Au, for instance, by contact with a 10-μM $NaBH_4$ solution for 30 s. The CN stretching band can then be observed at 2158 cm^{-1}, as shown in Figure 6(c), similar to that seen in Figure 6(b). On the other hand, the Fe^{2+}-bonded CN system on Au can be readily oxidized to the Fe^{3+}-bonded CN system on Au by contact with a 20-μM $KMnO_4$ solution for 30 s. The CN stretching band is then observed at 2180 cm^{-1}, as shown in Figure 6(d), similar to that seen in Figure 6(a).

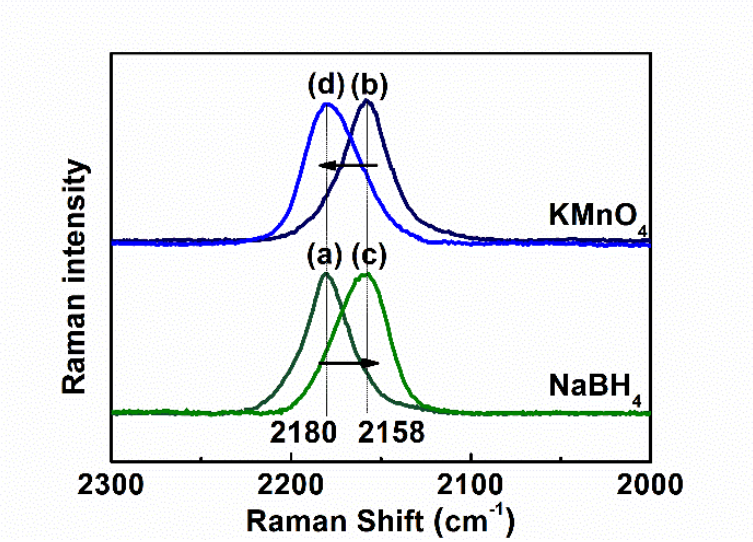

Figure 6. SERS spectra of (a) Fe^{3+}/NC/Au and (b) Fe^{2+}/NC/Au in as-prepared state, (c) Fe^{3+}/NC/Au after contact with a 10-μM $NaBH_4$ solution for 30 s, and (d) Fe^{2+}/NC/Au after contact with a 20-μM $KMnO_4$ solution for 30 s. All spectra were measured using 632.8-nm radiation as the excitation source.

2.4. Summary and conclusion

Highly SERS-active Ag and Au films were assembled not only onto a glass slide but also onto the inner surface of a glass capillary by adding toluene and BT (consecutively) to Ag and Au sol solutions prepared using PEI as both the reducing and stabilizing agent. The PEI-capped Ag and Au films were stable against cyanide etching and exhibited distinct CN stretching bands at 2132 and 2120 cm^{-1}, respectively, upon the adsorption of cyanide species. The pendant

nitrogen atom of the NC/Ag system, for instance, could form a dative bond with Fe^{3+} and Fe^{2+}, resulting in a blue-shift of the CN stretching band by as much as 27 and 11 cm^{-1}, respectively. The resulting Fe^{3+}/NC/Ag and Fe^{2+}/NC/Ag systems formed were stable under the laser light illumination at 632.8-nm. However, under the laser light illumination at 514.5-nm, the Fe^{3+}/NC/Ag system was gradually converted into the Fe^{2+}/NC/Ag system. This Fe^{3+} to Fe^{2+} conversion is due to the hot electrons generated from the PEI-capped Ag nanoparticle film. The Fe^{3+} to Fe^{2+} conversion was fitted to an exponential function, and the associated rate constant was confirmed to increase linearly with respect to the laser power at 514.5-nm. According to a temperature dependence study, the Fe^{3+} to Fe^{2+} conversion at 514.5-nm excitation was facile even at 77 K, suggesting that the plasmonic generation of hot electrons from the PEI-capped Ag nanoparticles is an efficient process. The infeasible oxidation of Fe^{2+} to Fe^{3+} was rationalized by arguing that hot holes, if generated, would be reactive only to the species in contact with Ag nanoparticles. On the other hand, as was the case for the Ag films, the Fe^{3+}/NC/Au and Fe^{2+}/NC/Au systems were invariant under the laser light illumination at 632.8-nm. Because the PEI-capped Au film was not SERS-active at 514.5-nm, we were unable to examine the possibility of the generation of hot electrons from the Au film using a laser light at shorter wavelengths. Instead, we confirmed that the Fe^{3+}/NC/Au system could be converted into the

Fe^{2+}/NC/Au system (or vice versa) by a brief contact with a mild solution of borohydride (or permanganate).

2.5. References

(1) Semenov, A. D.; Gol'tsman, G. N.; Sobolewski, R., *Supercond. Sci. Tech.* **2002,** *15*, R1.

(2) Roukes, M. L.; Freeman, M. R.; Germain, R. S.; Richardson, R. C.; Ketchen, M. B., *Phys. Rev. Lett.* **1985,** *55*, 422.

(3) Balkan, N., *Hot electrons in semiconductors : physics and devices*. Clarendon Press ; Oxford University Press: Oxford, New York, 1998; p xvi, 389 p.

(4) Wellstood, F. C.; Urbina, C.; Clarke, J., *Phys. Rev. B.* **1994,** *49*, 5942.

(5) Lindstrom, C. D.; Zhu, X. Y., *Chem. Rev.* **2006,** *106*, 4281.

(6) Petek, H.; Ogawa, S., *Prog. Surf. Sci.* **1997,** *56*, 239.

(7) Echenique, P. M.; Berndt, R.; Chulkov, E. V.; Fausterd, T. H.; Goldmann, A.; Hofer, U., *Surf. Sci. Rep.* **2004,** *52*, 219.

(8) Fang, Z. Y.; Liu, Z.; Wang, Y. M.; Ajayan, P. M.; Nordlander, P.; Halas, N. J., *Nano. Lett.* **2012,** *12*, 3808.

(9) Fang, Z. Y.; Wang, Y. M.; Liu, Z.; Schlather, A.; Ajayan, P. M.; Koppens, F. H. L.; Nordlander, P.; Halas, N. J., *Acs Nano.* **2012,** *6*, 10222.

(10) Knight, M. W.; Sobhani, H.; Nordlander, P.; Halas, N. J., *Science* **2011,** *332*, 702.

(11) Lee, Y. K.; Jung, C. H.; Park, J.; Seo, H.; Somorjai, G. A.; Park, J. Y., *Nano. Lett.* **2011,** *11*, 4251.

(12) Zhdanov, V. P.; Hagglund, C.; Kasemo, B., *Surf. Sci.* **2005,** *599*, L372.

(13) Douketis, C.; Haslett, T. L.; Shalaev, V. M.; Wang, Z. H.; Moskovits, M., *Physica. A.* **1994,** *207*, 352.

(14) Nolle, E. L.; Shchelev, M. Y., *Tech. Phys. Lett+.* **2004,** *30*, 304.

(15) Link, S.; El-Sayed, M. A., *J. Phys. Chem. B.* **1999,** *103*, 4212.

(16) Mulugeta, D.; Kim, K. H.; Watanabe, K.; Menzel, D.; Freund, H. J., *Phys. Rev. Lett.* **2008,** *101*, 146103.

(17) Redmond, P. L.; Wu, X. M.; Brus, L., *J. Phys. Chem. C.* **2007,** *111*, 8942.

(18) Kraeutler, B.; Bard, A. J., *J. Am. Chem. Soc.* **1977,** *99*, 7729.

(19) Kraeutler, B.; Bard, A. J., *J. Am. Chem. Soc.* **1978,** *100*, 5985.

(20) Mukherjee, S.; Libisch, F.; Large, N.; Neumann, O.; Brown, L. V.; Cheng, J.; Lassiter, J. B.; Carter, E. A.; Nordlander, P.; Halas, N. J., *Nano. Lett.* **2013,** *13*, 240.

(21) Han, S. W.; Lee, I.; Kim, K., *Langmuir* **2002,** *18*, 182.

(22) Kim, K.; Lee, I.; Lee, S. J., *Chem. Phys. Lett.* **2003,** *377*, 201.

(23) Lee, S. J.; Kim, K., *Chem. Phys. Lett.* **2003,** *378*, 122.

(24) Kim, K.; Lee, Y. M.; Lee, H. B.; Park, Y.; Bae, T. Y.; Jung, Y. M.; Choi, C. H.; Shin, K. S., *J. Raman. Spectrosc.* **2010,** *41*, 187.

(25) Kim, K.; Lee, J. W.; Shin, K. S., *Analyst* **2013,** *138*, 2988.

(26) Trainer, M.; Hsie, E. Y.; Mckeen, S. A.; Tallamraju, R.; Parrish, D. D.; Fehsenfeld, F. C.; Liu, S. C., *J. Geophys. Res.: Space Phys.* **1987,** *92*, 11879.

(27) Park, H. K.; Yoon, J. K.; Kim, K., *Langmuir* **2006,** *22*, 1626.

(28) Fleischm.M; Hendra, P. J.; Mcquilla.Aj, *Chem. Phys. Lett.* **1974,** *26*, 163.

(29) Norrod, K. L.; Sudnik, L. M.; Rousell, D.; Rowlen, K. L., *Appl. Spectrosc.* **1997,** *51*, 994.

(30) Chaney, S. B.; Shanmukh, S.; Dluhy, R. A.; Zhao, Y. P., *Appl. Phys. Lett.* **2005,** *87*, 31908.

(31) Hu, J. W.; Zhao, B.; Xu, W. Q.; Fan, Y. G.; Li, B.; Ozaki, Y., *Langmuir* **2002,** *18*, 6839.

(32) Kim, K.; Lee, H. B.; Lee, J. W.; Park, H. K.; Shin, K. S., *Langmuir* **2008,** *24*, 7178.

(33) Kim, K.; Lee, H. B.; Lee, J. W.; Shin, K. S., *J. Colloid. Interf. Sci.* **2010,** *345*, 103.

(34) Sun, X. P.; Dong, S. J.; Wang, E. K., *Langmuir* **2005,** *21*, 4710.

(35) Sun, X. P.; Dong, S. J.; Wang, E. K., *Polymer* **2004,** *45*, 2181.

(36) Sun, X. P.; Dong, S. J.; Wang, E. K., *Macromolecules* **2004,** *37*, 7105.

(37) Kim, K.; Lee, J. W.; Lee, H. B.; Shin, K. S., *Langmuir* **2009,** *25*, 9697.

(38) Kim, K.; Kim, K. L.; Choi, J. Y.; Shin, K. S., *Phys. Chem. Chem. Phys.* **2011,** *13*, 5981.

(39) Kim, K.; Kim, K. L.; Choi, J. Y.; Lee, H. B.; Shin, K. S., *J. Phys. Chem. C.* **2010,** *114*, 3448.

(40) Kim, K.; Shin, D.; Kim, K. L.; Shin, K. S., *J. Raman Spectrosc.* **2012,** *43*, 1427.

(41) Jacobs, M. B.; Jagodzinski, P. W.; Jones, T. E.; Eberhart, M. E., *J. Phys. Chem. C.* **2011,** *115*, 24115.

(42) Lu, X. M.; Au, L.; McLellan, J.; Li, Z. Y.; Marquez, M.; Xia, Y. N., *Nano. Lett.* **2007,** *7*, 1764.

국문 초록

본 연구에서는 유기 나이트릴 분자와 아이소나이트릴 분자의 표면 증강 라만 산란을 이용하여 CO 가 금 나노입자와 상호작용할 때의 전자 이동 방향, 그리고 가시광선에 의한 은 나노 구조체에서의 플라스몬 전자 방출 현상을 고찰하였다.

금과 은 나노 구조체에 흡착한 나이트릴 분자와 아이소나이트릴 분자의 CN 삼중결합 신축 진동 파동수는 나노 구조체의 표면 전하 (표면 전위)에 민감하다. 특히, 나이트릴 이온의 질소 비공유 전자쌍은 전이금속과 결합하여 CN 신축 진동 파동수를 변화시켜 낮은 농도까지 효과적으로 검출 가능하다.

이러한 특징을 가지는 분자들을 이용하여, 1 장에서는 표면 증강 라만 활성인 금 기질에 2,6-디메틸페닐아이소시아나이드를 흡착시킨 후에 일산화탄소를 노출시키면 금에서 CO 로 전자가 이동하여 금 기질의 표면 전위가 증가하게 됨을 NC 신축 진동 파동수의 청색 이동으로 확인할 수 있었다.

2 장에서는 표면 증강 라만 산란 활성인 금과 은 나노 필름에 나이트릴을 흡착시킨 후 철 3 가와 철 2 가 이온을 나이트릴 이온의 질소 비

공유 전자쌍에 결합하면 CN 신축 진동수가 달리 나타나는데, 514.5 nm 의 빛을 쪼이면 Ag 에서 플라스몬 전자가 방출되어 철 3 가 이온이 철 2 가 이온으로 환원되는 것을 CN 신축 진동수의 변화를 통해 확인할 수 있었다.

주요어: 2,6-디메틸페닐아이소시아나이드, 나이트릴, 일산화탄소, 은, 금, 표면 증강 라만 산란, 표면 전위, 열 전자, 플라즈모닉스

학번: 2012-20284